SAND2017-5038C

Electrical and X-ray diagnostics on the NSTec 2-MA dense plasma focus system[§]

M.E. Savage[1], O. Johns[1], M. Garcia[1], P. Lake[1], J.K. Moore[1], E. Ormond[1], T.J. Webb[1], N. Bennett[2], B. Gall[2], S. Gardner[2], S. Molnar[2], N. Sipe[2], T. Weber[3], R.T. Olson[3], A. Schmidt[4]

[1]Sandia National Laboratories, Albuquerque NM 87185

[2]NSTec, Las Vegas NV

[3]Los Alamos National Laboratory, Los Alamos NM

[4]Lawrence Livermore National Laboratory, Livermore CA

National Security Technologies (NSTec) is developing dense plasma focus (DPF) systems for applications requiring intense pulsed neutron sources. Sandia National Laboratories participated in a limited number of experiments with one of those systems. In collaboration with NSTec, Los Alamos National Laboratory, and Lawrence Livermore National Laboratory, we installed additional electrical and X-ray image measurements in parallel with normal operation of the system. Dense plasma focus machines have been studied for decades, but much of the experimental interest has been on neutron and X-ray yield. The primary goal for the present work was to develop and field high-fidelity and traceably-calibrated current and voltage measurements for comparison to digital simulations. The secondary goals were to utilize the current and voltage measurements to add general understanding of vacuum insulator behavior and current sheath dynamics. We also conducted initial scoping studies of soft X-ray diagnostics. We will show the electrical diagnostics and the techniques used to acquire high-fidelity signals in the difficult environment of the 2 MA, 6 μs plasma focus drive pulse. We will show how we measure accreted plasma mass non-invasively, and the sensitivity to background fill density. We will present initial qualitative results from filtered X-ray pinhole images and spectroscopic data from the pinch region.

I. The dense plasma focus system

The coaxial dense plasma focus has been studied and used to generate pulsed radiation (X-rays and neutrons) since the 1960s. Devices using stored energies ranging from a few joules, to megajoules, have been built. [1-7]

The dense plasma focus could be considered a compact combination of an electrical pulse compression system and a gas z-pinch load. Operating a dense plasma focus device is simple. Initially, a static gas fill (often including deuterium for neutron production) is admitted into the vacuum chamber encompassing the DPF electrodes, at typical pressures of a few Torr. A voltage is then applied to the electrodes from a (typically DC-charged and spark-gap switched) kilovolt capacitor bank. A discharge occurs at the breech end of the system, along the vacuum insulator surface.

As current increases, the power flow circuit accumulates magnetic energy. The current path includes a moving radial current plasma sheath between the coaxial electrodes. Magnetic pressure drives the current sheath axially from the breech end of the coaxial system, snowplowing through the neutral gas fill, towards the load region. The gas fill pressure and the electrode geometry are configured so that near peak current in the system, the sheath reaches the load end of the electrodes. The time for the axial translation can be several microseconds, and is variable over a wide range to match the capacitor bank by adjusting the static fill pressure.

At the end of the coaxial section, the current sheath motion is forced to transition from axial to radial, and the inductance increases significantly. Because of the dynamic inductance increase and the current flowing, a transient voltage greater than the initial capacitor voltage can be applied to the load. This necessarily shortens the load pulse duration and increases the power dissipated in the load. The plasma mass density and magnetic energy density are both increased due to radial compression. In many devices, the voltage and current are both high enough to generate significant neutron and X-radiation.

The NSTec system on which these experiments were done utilizes a 432 μF capacitor bank storing 265 kJ at a (typical) ±17.5 kV charge voltage.[8] The drive capacitor bank inductance is about 40 nH. With a plasma load, peak current is typically more than 2 MA and occurs ~6 μs after triggering the capacitor bank switches. The experiments described here used pure deuterium gas fill in the DPF.

II. Electrical measurements

A dense plasma focus is an electrical system, and we consider accurate current and voltage measurements to be fundamental. Current and voltage in the dense plasma focus can be measured with conventional techniques. Aspects of the system make the measurements somewhat challenging because of the high peak current and the long rise time. In addition, the new diagnostics had to be retrofitted into the already-built system.

[§] Sandia National Laboratories is a multimission laboratory managed and operated by National Technology and Engineering Solutions of Sandia, LLC., a wholly owned subsidiary of Honeywell International, Inc., for the U.S. Department of Energy's National Nuclear Security Administration under contract DE-NA-0003525.

Figure 1 shows the basic layout of the NSTec DPF system. The DPF anode diameter is 7.6 cm, the cathode diameter is 10.2 cm, and the overall diameter is 1.2 meters. The electrodes in vacuum are made of copper.

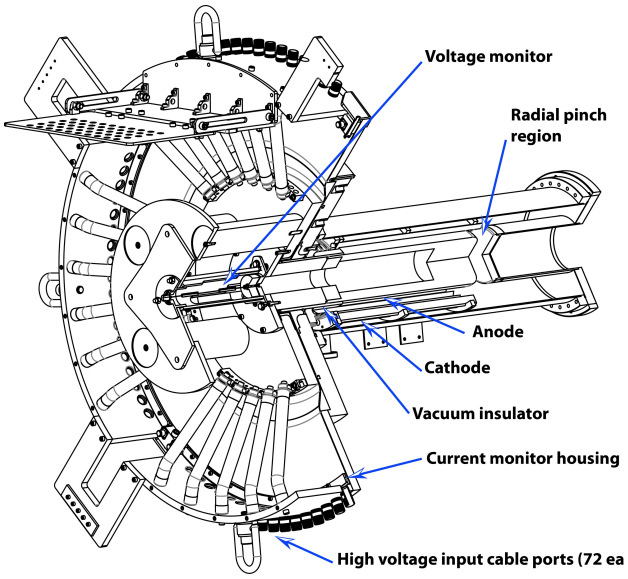

Figure 1. Sectional view of the NSTec DPF system with the additional electrical diagnostics shown. The 72 high voltage power feed cables from the capacitor bank are not shown.

All the additional signals traveled through 5/8-inch diameter Heliax [9] cable from the DPF itself to the diagnostic enclosure. The -3dB bandwidth of the nine-meter cable runs is of order 3 GHz, but that is not the reason this cable was chosen. This relatively large-diameter cable has a solid copper outer conductor and among the lowest DC shield resistance values (per unit length) of readily available 50Ω cable. The slow current rise time of the DPF can allow magnetic flux from stray current to penetrate signal cables (because of ground conductor resistance), manifesting itself as common–mode spurious signals. In a low-impedance slow system such as the DPF, magnetic flux penetration can be a significant signal noise source. In addition, the AC power to the acquisition enclosure was isolated with a low-capacitance transformer to minimize ground loop currents and passed through a commercial power filter.

Typically, during a pulsed power discharge event, the signal level from the diagnostics decreases with time in the pulse; concurrently the spurious noise level increases with time. Because of that, the signal-to-noise ratio of electrical measurements decreases in time, often exponentially with an *e*-folding constant given largely by the effective cable plant inductance divided by the effective signal cable plant ground shield resistance. Maximizing the noise-encroaching time constant (as much as is practical) is often the most effective way to improve the signal-to-noise ratio. A noise time constant of 2 μs is typical in pulsed power experiments, but the slow DPF pulse here requires much longer noise-exponentiating times for high-fidelity data throughout the entire time of interest.

The signals were acquired on calibrated Tektronix TDS digitizers. Signal levels were reduced to ~1V inside the acquisition enclosure with calibrated high-quality attenuators designed for pulsed signals. The digitizers were externally triggered by a signal from the DPF control system. The data acquisition software allows correction for cable length, attenuation, compensation for cable dispersion if desired, and extensive post-processing of waveform data.

A. Current measurement

The electrical current measurement was in air, outside the vacuum insulator. Concepts to measure current in vacuum, downstream of the vacuum insulator were considered, but limited experimental time precluded testing.

The current measurement was done with a segmented Rogowski configuration. Such distributed flux probes [10-12] are commonly used in dense plasma focus and other systems. The current monitors used here produce a signal in the time-derivative mode to maximize the signal level (and hence signal-to-noise ratio). The magnitude of the output voltage from a diagnostic is the most significant general difference between self-integrating and derivative-responding current (or voltage) monitors. To the extent that integration (numerical or otherwise) and frequency-dependent cable attenuation are both linear processes, whether the signal of interest or its derivative passes through the signal cable run has absolutely no effect on the overall frequency response.

Eight individual 45-degree segments of the current feed perimeter (1.14m diameter) are recorded individually. This reduces the effective length (transit time) of the diagnostic, [13] improving the high-frequency response, as well as providing some spatial resolution and, (with alternating signal polarities), a degree of common mode noise rejection. The individual current monitor signals are numerically integrated and combined in post-processing.

The current monitors were calibrated in-situ against a NIST-traceable, 2.5 ns rise time current transformer (Pearson 6595). [14] For calibration, a low energy, low impedance pulse generator drove ~5 kA peak current (at 2×10^{11}A/s) through the reference current transformer and the diagnostic monitors being calibrated. Current flow during calibration was from the pinch end of the DPF towards the capacitor bank, through the same path as would be driven from the capacitor bank and high-voltage cables (albeit in the opposite direction). This compensates the calibration data for geometry-specific effects on current flow.

The fastest DPF current transition time observed or predicted in the system being studied is of order 100 ns. The calibration pulse current rise time was 30 ns. The rise time of the numerically integrated monitor signals from the calibration pulse is indistinguishable from the rise time of

the current transformer reference signal. We conclude that the rise time of the DPF-current diagnostic is 15 ns or less, and therefore adequate to resolve any features in the DPF current waveform. Figure 2 shows total current measured with the segmented Rogowski probe on a typical ±17.5kV bank charge plasma experiment.

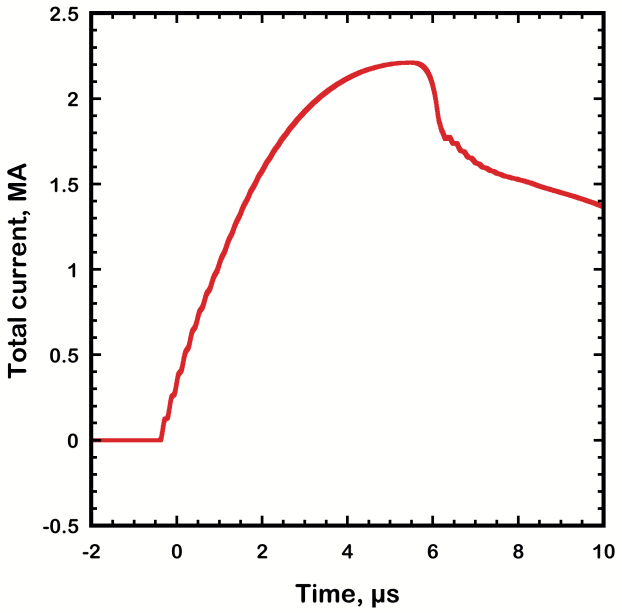

Figure 2. Typical measured total DPF current with a normal plasma load. Zero time is when the trigger signal reaches the acquisition enclosure and is not tied to a specific phase of the DPF evolution.

B. Voltage measurement

A single voltage monitor was implemented on the DPF. This measurement was also in air, upstream of the vacuum insulator. Exploiting symmetry, the voltage diagnostic was located on the rotational axis centerline of the DPF. Symmetry and the high impedance design of the monitor reduce the contribution from changing magnetic flux to a negligible level.

The voltage monitor consists of four precision, low-voltage-coefficient resistors in a series string. Excessive energy deposition in these resistors could cause permanent changes in resistance. For this reason, a series blocking capacitor restricts the duration high voltage could be applied to the monitor resistors in case of delayed DPF current initiation. Even if there were no other load apart from the voltage monitor, the series capacitor would limit the energy deposited in each resistor to less than one Joule, a safe value. In experiments observed to date, the DPF current consistently begins within 30 nanoseconds after voltage application and resistor dissipation is negligible; however, we have left the capacitor installed in case of a future anomaly.

The monitor resistance was calibrated with a traceable ohmmeter. The resistance value was 3.93kΩ and the blocking capacitance value was 2.6 nF. The "droop" time-constant effect on the monitor signal is therefore ~10 μs and has a noticeable impact on the uncompensated waveform. The strontium-titanate blocking capacitor charges to less than 10 kV during a normal pulse; the total capacitance change due to voltage is less than 1%. The compensation for the capacitor droop is a simple (and analytically exact) waveform calculation step that is essentially transparent in the data processing.

Inductance of the resistor string is not a limiting issue, because of the short inductive time constant resulting from the relatively large resistance. More important for a high impedance divider is shunt capacitance of the resistors. The design of this monitor was chosen such that the L/R and RC (series-inductive and shunt-capacitive) time constants are both sub-nanosecond. The signal level from the voltage diagnostic is ~1kV peak.

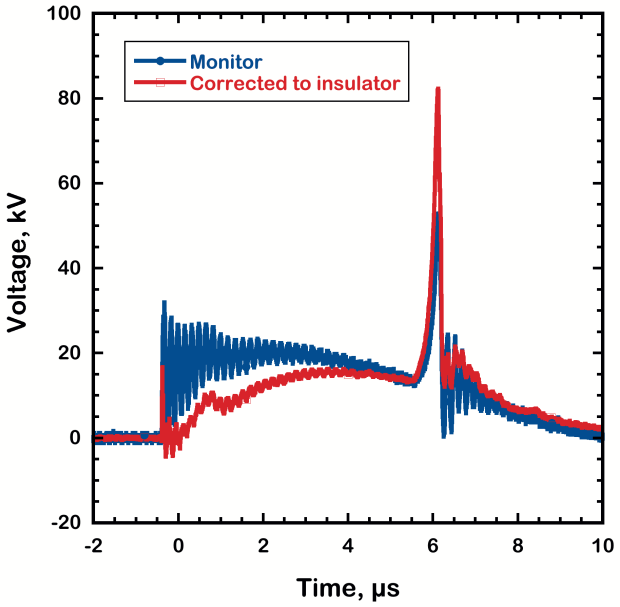

Figure 3. Voltage at the monitor location, and voltage corrected to the vacuum insulator location with a transmission line model.

Because the DPF is a slow (current rise time much larger than wave transit time through the system) and low-impedance device, at a given time the current is nearly constant throughout the system. Voltage, however, can vary significantly. This is shown in Figure 3. The (droop-corrected) voltage monitor signal is shown, as well as corrected voltage translated to the vacuum insulator location. The translation is done using a simple transmission line model [15] utilizing the measured current, the TEM wave transit time and the average TEM transmission line impedance between the voltage monitor location and the vacuum insulator. The damped oscillation in the waveforms is physically real and is caused by the interaction of the capacitor bank inductance with the capacitance of the high voltage cables connecting the capacitor bank to the DPF.

The voltage extrapolated to the vacuum insulator location is significantly different from the voltage

measured at the monitor. Typically, voltage at the vacuum insulator position is more useful for studying machine performance and analyzing data than is voltage at the monitor location. The voltage extrapolation calculation is simple and analytically exact.

III. Analysis

It is possible to study DPF performance at a basic level with voltage and current diagnostics alone. The techniques shown here are straightforward but not prevalent in the literature. The analysis requires basic manipulation of the waveform data. The first step, as shown previously, is to compute voltage at the vacuum insulator.

Further processing can be compared to simple plasma modeling of fundamental DPF behavior. Because the DPF is a low-impedance system with most of the energy in magnetic field, time-dependent system inductance is a useful calculation. With no assumptions other than a relatively low resistive voltage drop in the plasma sheath, inductance can be easily calculated.[16] This is done with the relation

$$L_{vacuum} = \frac{1}{I}\int_{-\infty}^{t} V_{insulator} d\tau \qquad (1)$$

where L_{vacuum} is the inductance downstream of the vacuum interface, I is the current flowing into the vacuum interface, and $V_{insulator}$ is the voltage at the vacuum insulator. This calculated inductance would be expected to be greater than zero before insulator flashover, approximately zero immediately after surface breakdown, and then rise as magnetic pressure drives the current sheath away from the insulator and axially downstream. The inductance should rise abruptly when the sheath reaches the axial extent of the electrodes and begins the radial pinching. The voltage peak (at 6 μs in Figure 3) occurs when the inductance is increasing rapidly (Figure 4).

The geometry of the DPF electrodes determines the inductance increase as the current sheath translates. We will assume *a priori* that the current flow is two-dimensional, or at least comprised of multiple spokes. We also assume that current flow is largely radial with an axial position centroid represented by the inductance, although some axial shear to the sheath is possible due to the higher magnetic field at the center conductor.

For convenience, we will use the free-space vacuum impedance of the electrode system instead of the inner and outer radii. We will also neglect the inductance increase caused by the 24 discrete rods in the cathode structure (~3 nH total, or 10%) because we expect that plasma may not be ejected fully from the azimuthal gaps between rods. The wave impedance value thus calculated is 17.3Ω for the NSTec electrodes. The axial length of the electrodes is 58 cm, or 1.9 ns axial transit time. The inductance increase from initiation to the radial pinch phase should therefore be 33.5 nH if plasma were completely cleared from the gap behind the current sheath. In Figure 4, the second-derivative inflection to the higher inductance change rate (presumed to be associated with the start of the radial pinch phase) happens at 32.9 nH. Shunt losses (e.g., at the vacuum insulator) would decrease the calculated inductance by increasing the current. Because of the agreement with the geometric inductance calculations, we conclude that shunt losses are not significant.

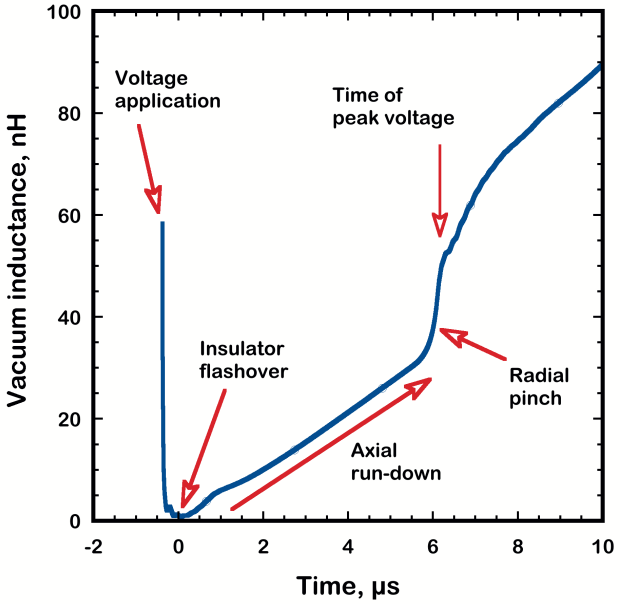

Figure 4. Inductance downstream of the vacuum insulator. The inductance should start higher than zero before current flows, then approach zero as the sheath bridges the insulator. Inductance increases as the current sheath begins translating away from the insulator.

The DPF dynamic inductance observed is notionally consistent with a nominally two-dimensional current sheath. Following Hart [17, 18] we find that the magnetic force on the current sheath is a function only of the current and the vacuum wave impedance. A convenient form of the total axial magnetic force expression, valid for any axially symmetric current distribution, is

$$Force = \frac{Z_{vacuum}}{2c} I^2 \qquad (2)$$

where $Force$ is the total axial magnetic force on the sheath, Z_{vacuum} is the vacuum wave impedance of the coaxial structure, c is the speed of light in vacuum, and I is the sheath current.

We can equate the magnetic force to the change in momentum of the current sheath,

$$\frac{d}{dt}(mv) = \frac{Z_{vacuum}}{2c} I^2 \qquad (3)$$

where m is the total plasma mass, and v is the sheath velocity. The axial sheath velocity can be written

$$v = \frac{dL}{dt}\frac{\Delta x}{\Delta L} \qquad (4)$$

where Δx is the total axial translation distance and ΔL is the total inductance of the axial region. The sheath axial velocity in terms of the inductance increase rate is

$$v = \frac{dL}{dt}\frac{c}{Z_{vacuum}} \qquad (5)$$

The expression for the accumulating plasma mass during axial translation as a function of time is then

$$m = \frac{{Z_{vacuum}}^2}{2c^2\frac{dL}{dt}}\int_{-\infty}^{t} I^2 d\tau \qquad (6)$$

The expression for accreted mass can be easily evaluated using experimental data, and plotted against axial distance. This is comparable to the form presented by Mather.[19]

For comparing the calculated accreted mass to that expected from the neutral gas fill, the density of deuterium gas is readily calculated to be 235 ng/cm^3/Torr. The total neutral gas mass is 1.94 mg/Torr of deuterium, given the 142 cm^2 sheath area and 58 cm axial length of the NSTec DPF.

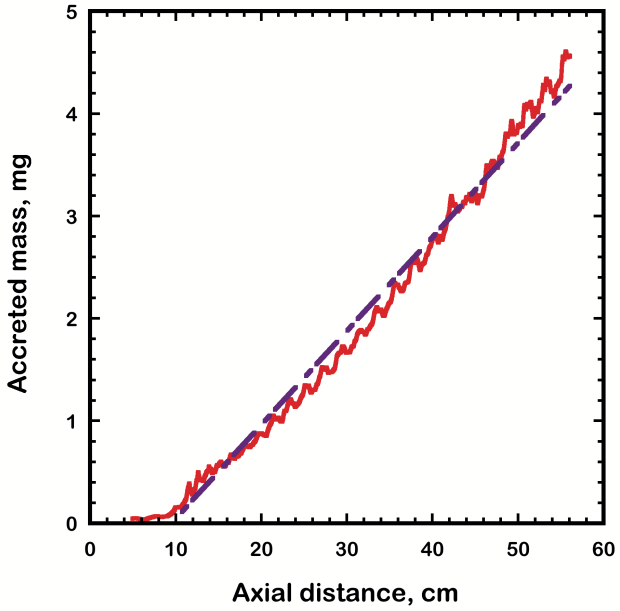

Figure 5. Calculated accreted plasma current sheath mass at 4.5 Torr deuterium fill versus distance from the breech end of the DPF. The calculation stops at 58 cm where the radial pinch begins. The line shown is a least-squares fit to the data.

The computed plasma mass versus axial distance from the breech is shown in Figure 5 for an experiment at 4.5 Torr deuterium fill. The analysis shown ignores radial sheath motion, which may be important during the current sheath lift-off from the insulator surface (the insulator is 10cm long). The line shown in Figure 5 is a least-squares fit to the mass data. The slope of the fit curve is 0.092 mg/cm, and the neutral gas density is 0.15 mg/cm. The measured mass accretion rate is 39% lower than the background fill density. Some of the difference is likely due to an angled current sheath, which provides a radially outward component to the sheath velocity, and could eject some of the accreted mass. [18]

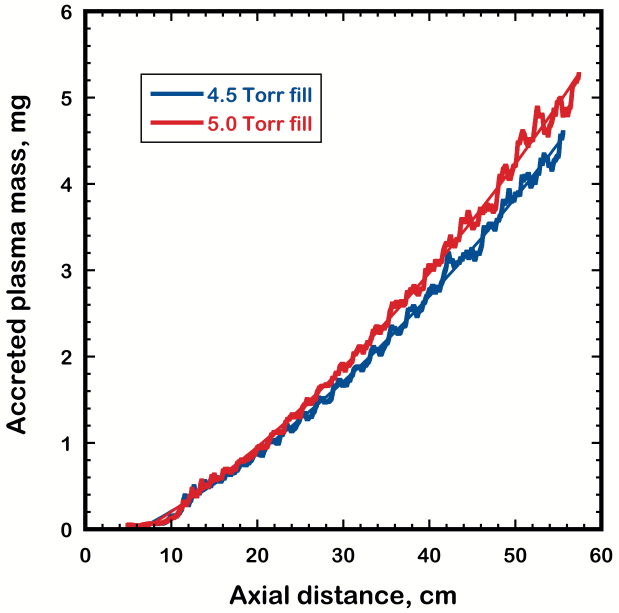

Figure 6. Calculated accreted mass for two nominally identical tests, one at 4.5 Torr deuterium, and one at 5.0 Torr deuterium. The calculated mass difference is consistent with the change in fill density.

Recent work with a different mass measurement technique [20] and a higher aspect-ratio axial section, show a measured accreted mass 94% lower than the neutral fill density. In another experiment, [21] analysis similar to that used here but with a somewhat larger aspect ratio ($Z_{vacuum} = 24\Omega$) in an argon-filled device, showed a mass accretion deficit (inferred from sheath velocity) of 44%. In a 13 kJ deuterium system with 42Ω electrode geometry and assuming a constant 10cm/μs sheath velocity, Mather shows a mass accretion deficit of 21%. [19]

If the calculation is truly representative of the accreted mass, then there should be a difference with background fill gas pressure. To test this, we conducted nominally identical experiments at 4.5 Torr neutral gas fill and 5.0 Torr gas fill. Figure 6 shows calculated accreted mass for those discharges. A least-squares fit between the calculated mass curves for the two experiments yields a 1.12 mass ratio; the expected ratio based on the measured fill pressures is 1.11.

The accreted mass measurement is sensitive to material desorbed from the electrodes as well as the static gas fill. As a further demonstration of the utility of waveform processing, we can compare the mass calculated on a nominal test (e.g., Figure 5) to mass data from an unconditioned experiment. The DPF is normally operated without exposing the vacuum electrodes to atmosphere. Without one or more conditioning discharges, the DPF system rarely produces indications of normal radial pinching.

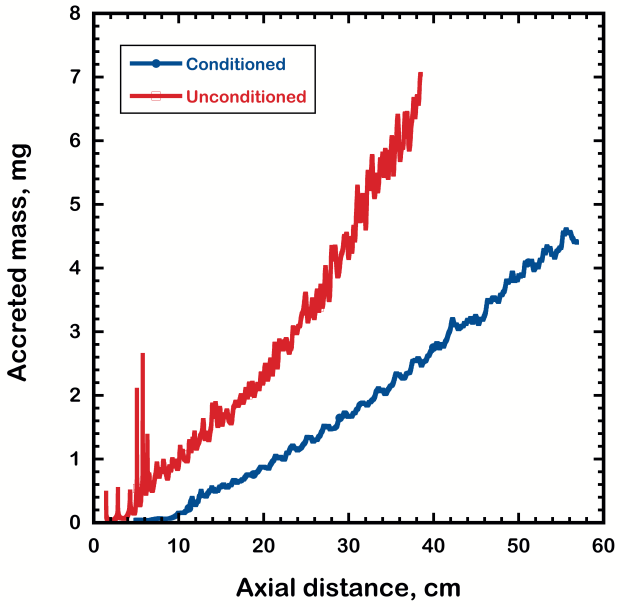

Figure 7. Calculated accreted mass from 1) an experiment after multiple conditioning shots (blue line), and 2) the first discharge after exposing the DPF electrodes to humid atmosphere (red line). In the unconditioned test, the accreted mass is higher throughout the current rise time, and it appears that the current sheath never reached the end of the coaxial electrodes (58 cm) in the waveform record. No neutrons were observed on the unconditioned experiment.

The NSTec DPF system is located in an evaporatively cooled facility, and during summer the ambient humidity in the laboratory is high. Appreciable water contamination of the unbaked electrode surfaces exposed to humid laboratory air is possible. Waveforms were acquired on the first discharge after exposing the DPF electrodes to humid atmosphere ("unconditioned"), and again several discharges later ("conditioned"). Figure 7 shows the results of mass calculations on the data. Both conditioned and unconditioned experiments were done with 4.5 Torr of pure deuterium neutral gas fill, the same electrodes, and the same charge voltage. The unconditioned test indicates triple the mass density throughout the current rise, and consequently, failure to reach the end of the axial translation region in the usual time.

IV. X-ray diagnostics

A limited amount of work was done to investigate X-ray data from the plasma focus device. Issues of interest were whether contaminates could be detected in the hot deuterium plasma, which could help identify the source of extraneous material. The initial testing was a qualitative survey of the X-ray intensity levels and the brightest spectral lines. The data were acquired with image plates on single discharges of the DPF system.

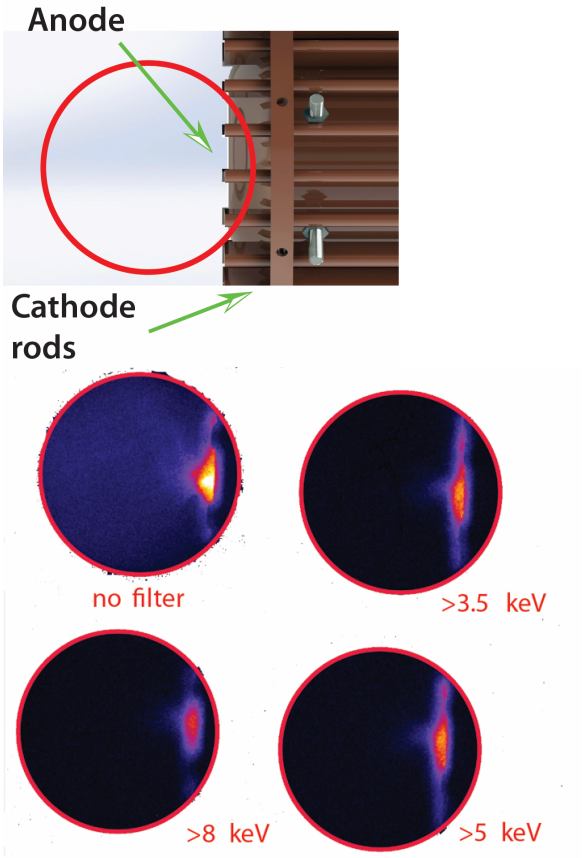

Figure 8. (Upper) Image of pinhole camera field of view [circle]. (Lower) Time-integrated, energy-filtered X-ray images of a dense pinch discharge. Energy cuts shown are e-folding values.

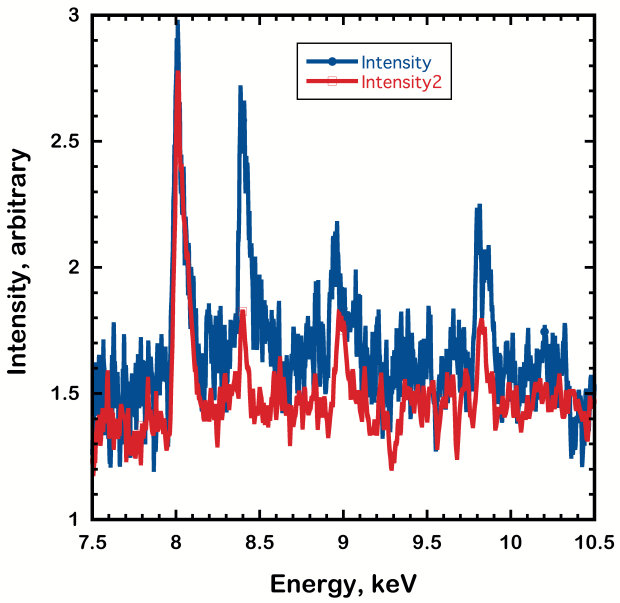

Figure 9. Time-integrated X-ray spectra from the anode and plasma in the pinch region on two experiments. Copper transition lines at 8.048, 8.39, 8.9 and 9.87 keV are present.

Figure 8 shows multiple time-integrated images at with no filter, 3.5 keV (e-fold) energy, 5 keV, and 8 keV high-pass filter attenuation e-folding energies. The image views the anode face and the expected pinch region. As expected, the highest X-ray energy emanates from the copper anode, but detectable radiation above 3.5 keV is evident from the plasma pinch.

A time-integrated bent-crystal spectrometer was also used on a test, looking at the anode face and plasma pinch region. Figure 9 shows results from a LiF spectrometer viewing the pinch radially. No attempt was made to obscure the copper anode face.

V. Summary

A small number of experiments on a 2-MA dense plasma focus were done with the goal of accurate electrical measurements. The electrical data are consistent with simple models of the current sheath. We developed a simple model for calculating plasma mass using only conventional voltage and current diagnostics. It appears possible to discern mass variations of 10% or less and may help identify causes of low radiation yield experiments.

Preliminary and qualitative soft X-ray measurements show copper line emission presumably from the anode surface and indications of X-ray energies above 3.5 keV being emitted from the pinch plasma.

VI. Acknowledgments

The authors would like to thank the entire NSTec group for outstanding support of these experiments done in addition to their other commitments. The authors would also like to thank Dr. Rick Spielman for enlightening discussions of plasma focus work, and development of circuit modeling tools. We would thank Drs. M.E. Cuneo and W.A. Stygar for Sandia management support of the effort.

VII. References

1 M. Krishnan, "The Dense Plasma Focus: A Versatile Dense Pinch for Diverse Applications" Plasma Science, IEEE Transactions on **40**, 3189 (2012).

2 H. Krompholz, F. Rühl, W. Schneider, K. Schönbach, and G. Herziger, "A scaling law for plasma focus devices" Physics Letters A **82**, 82 (1981).

3 J. W. Mather, "Investigation of the high-energy acceleration mode in the coaxial gun" Physics of Fluids **7**, S28 (1964).

4 J. W. Mather, "Formation of a high-density deuterium plasma focus" Physics of Fluids **8**, 366 (1965).

5 D. W. Price, AFWL Internal Report, "Bibliography of documents related to the theory, operation and performance of coaxial plasma guns", AFWL-TR-88-72, 1988

6 M. Scholz, B. Bieńkowska, M. Borowiecki, I. Ivanova-Stanik, L. Karpiński, W. Stępniewski, M. Paduch, K. Tomaszewski, M. Sadowski, *et al*., "Status of a mega-joule plasma-focus experiments" Nukleonika **51**, 79 (2006).

7 V. Tang and B. Rusnak, Lawrence Livermore Internal Report, "Review of dense plasma focus technology for intense and directional neutron sources", LLNL-TR-401857, 2008

8 N. Bennett, M. Blasco, K. Breeding, D. Constantino, A. DeYoung, V. DiPuccio, J. Friedman, B. Gall, S. Gardner, *et al*., "Development of the dense plasma focus for short-pulse applications" Physics of Plasmas **24**, 012702 (2017).

9 www.commscope.com.

10 D. G. Pellinen, M. S. D. Capua, S. E. Sampayan, H. Gerbracht, and M. Wang, "Rogowski coil for measuring fast, high-level pulsed currents" Rev. Sci. Instrum. **51**, 1535 (1980).

11 W. Stygar and G. Gerdin, "High Frequency Rogowski Coil Response Characteristics" IEEE Transactions on Plasma Science **10**, 40 (1982).

12 S. Lee, S. H. Saw, R. S. Rawat, P. Lee, R. Verma, A. Talebitaher, S. M. Hassan, A. E. Abdou, M. Ismail, *et al*., "Measurement and Processing of Fast Pulsed Discharge Current in Plasma Focus Machines" Journal of Fusion Energy **31**, 198 (2012).

13 J. Cooper, "On the high-frequency response of a Rogowski coil" Plasma Physics (Journal of Nuclear Energy Part C) **5**, 285 (1963).

14 www.pearsonelectronics.com.

15 M. E. Savage, J. C.W. Mendel, T. W. Grasser, W. W. Simpson, and D. M. Zagar, "Time-resolved voltage measurements in terawatt magnetically insulated transmission lines" Review of Scientific Instruments **61**, 3812 (1990).

16 H. Bruzzone, H. Acuña, M. Barbaglia, and A. Clausse, "A simple plasma diagnostic based on processing the electrical signals from coaxial discharges" Plasma Physics and Controlled Fusion **48**, 609 (2006).

17 P. J. Hart, "Plasma Acceleration with Coaxial Electrodes" Physics of Fluids **5**, 38 (1962).

18 P. J. Hart, "Modified snowplow model for coaxial plasma accelerators" J. Appl. Phys. **35**, 3425 (1964).

19 J. W. Mather, in *Methods of experimental physics*, edited by L. Marton (Academic Press, New York, 1971), Vol. 9B, p. 187.

20 L. S. Caballero Bendixsen, S. C. Bott-Suzuki, S. W. Cordaro, M. Krishnan, S. Chapman, P. Coleman, and J. Chittenden, "Axial mass fraction measurements in a 300kA dense plasma focus" Physics of Plasmas **23**, 093112 (2016).

21 S. Al-Hawat, "Axial velocity measurement of current sheath in a plasma focus device using a magnetic probe" IEEE Transactions on Plasma Science **32**, 764 (2004).